A Theoretical Investigation on the Properties of the New Poly(*N*-vinylcarbazole)-3-Methylthiophene (PVK-3MeT) Synthesized Graft Copolymer

Mourad Chemek,[1] Sahbi Ayachi,[1] Abdelkader Hlel,[1] Jany Wéry,[2] Serge Lefrant,[2] Kamel Alimi[1]

[1]*Unité de recherche : Matériaux Nouveaux et Dispositifs Electroniques organiques, Faculté des Sciences, Université de Monastir, 5000, Tunisie*
[2]*Institut des Matériaux Jean Rouxel, CNRS-UMR 6502, 2 Rue de la Houssinière, BP 32229, 44322 Nantes Cédex 3, France*

Received 18 October 2010; accepted 8 February 2011
DOI 10.1002/app.34328
Published online 17 June 2011 in Wiley Online Library (wileyonlinelibrary.com).

ABSTRACT: In this article, we present quantum chemical calculations, based on density functional theory (DFT), performed to investigate the geometries and the opto-electronic properties of a new synthesized graft copolymer based on poly(*N*-vinylcarbazole) (PVK) and poly(3-methylthiophene) (PMeT) named PVK-3MeT. First, we have theoretically computed and compared the structural, optical, and vibrational parameters of both neutral and doped states. In addition, the excited state was theoretically obtained by the *ab initio* RCIS/STO-3G method. To assign the absorption and emission peaks observed experimentally, we computed the energies of the lowest singlet excited state with the time-dependent density functional theory (TD-DFT) method. Electronic parameters such as the HOMO-LUMO band gap, the ionization potential (IP), and electron affinity (EA) are extracted. Calculations show that the PVK-3MeT copolymer is nonplanar in its ground neutral state. Meanwhile, upon doping or photoexcitation, an enhancement of the planarity is observed, resulting on a decrease of the inter-ring torsion angle between 3-methylthiophene units. Such modifications in the geometric parameters induce a dramatic change on the HOMO and LUMO orbitals in the doped or excited states.
 J Appl Polym Sci 122: 2391–2402, 2011

Key words: calculations; density functional theory (DFT); graft copolymers; structure-property relations

INTRODUCTION

Nowadays, organic materials based on conjugated polymers present a new area of research, in both experimental and theoretical chemistry and physics, due to their interesting optoelectronics properties, as well as to their easy and low-cost processing.[1–4] Consequently, organic materials based on conjugated polymers are attractive candidates to be used as active layers in optoelectronic devices, such as polymer light emitting diodes (PLEDs) and organic sensors.[5–7] The wavelength emitted from PLEDs is directly depending on the extent of conjugation in the polymer, and therefore short conjugation systems emit rather in the blue while long conjugation ones emit in the red range.[8,9] Consequently, it exist close relation-ships between the chemical structure of the conjugated polymers and their optical properties. As a consequence, the prediction of the optical properties of such polymers is still a real challenge. In this context, combining quantum chemical calculations and spectroscopic characterization studies can lead to a better understanding of the correlation between structure and properties of a new organic synthesized polymer. Moreover, density functional theory (DFT) has proved to be successful in predicting and reproducing geometrical and optoelectronic properties of a variety of organic compounds, and in addition, more accurate than semi empirical and *ab initio* methods.[10–12]

Recently, we have chemically synthesized and characterized by various experimental spectroscopic techniques a new graft copolymer based on poly (*N*-vinylcarbazole) (PVK) and poly(3-methylthiophene) (PMeT). Two samples named PVK-3MeT1 and PVK-3MeT2 were prepared with two different polymerization yields, in the doped and chemically de-doped states.[13]

To rationalize the experimental properties of the synthesized graft copolymer and to predict those of unknown ones, the theoretical investigation of the structure, electronic and emissive properties of this new material is needed, especially for the geometric parameters and characteristic optoelectronic parameters such as the high occupied molecular orbital (HOMO) and lowest unoccupied molecular orbital (LUMO) energies, ionization potential (IP), and

Correspondence to: K. Alimi (kamel.alimi@fsm.rnu.tn).
Contract grant sponsor: Tunisian-French cooperative action; contract grant number: CMCU/07G1309.

electron affinity (EA), difficult to obtain experimentally. Here, we report the structural and the optoelectronic properties of the graft copolymer obtained from the two synthesized samples, in the ground neutral, doped and excited states, using density functional theory (DFT), time-dependent density functional theory (TD-DFT), and the configuration interaction singles (CIS) methods. The aim of the present work is to provide a clear understanding and description of the geometrical parameters and the optoelectronic properties of the synthesized copolymer. The theoretical predictions are compared to the available experimental data[13] for a reliable description of the PVK-3MeT properties, to predict the potential optoelectronic applications for this new organic material.

COMPUTATIONAL DETAILS

The molecular quantum chemical calculations were performed essentially using the framework of the Kohn-Shan Density Functional Theory (DFT)[14] implemented in the Gaussian 03 program package.[15] All calculations on the studied oligomer of this work were done on cluster machines in the CCIPL (Intensive Computing center at the University of Nantes (Pays de la loire)). The investigated polymers correspond to the chemically synthesized copolymers named PVK-3MeT1 and PVK-3MeT2, mentioned above and described in our previous article.[13] To facilitate the simulation and to reduce the time of calculation, *N*-vinylcarbazole has been replaced by carbazole unit. As a matter of fact, it has been proved that the presence of aliphatic group (alkyl, methyl, vinyl..) does not significantly affect the equilibrium in the geometry as well as the electronic and the optical properties.[16,17]

The geometrical structure of the copolymer (Scheme 4) has been firstly optimized for the neutral ground state using the spin-restricted RDFT for the open shell system with the Beckee three-parameter exchange functional with nonlocal correlation provided by the Lee-Yang-Parr method, denoted B3LYP,[18,19] and the Becke's three-parameter hybrid functional combined with the nonlocal correlation provided by Perdew and Wang's (PW91), denoted B3PW91,[20,21] combined with 6-31G (d) basis set. Meanwhile, the doped state was obtained by optimization of the molecular structure in the spin-unrestricted closed shell system UDFT, frequently used for the description of the radical or biradical (doped) state,[22,23] with the B3LYP and B3PW91 methods, combined with 6-31G (d).

On the fully geometry optimized structure, the ground and excited-state energies were then investigated using time-dependent density functional theory (TD-DFT) method at the RB3LYP and RB3PW91, for the ground neutral state and by TD-DFT/UB3LYP and TD-DFT/UB3PW91, for the doped state using 6-31G (d) as a basis set. Furthermore, simulated vibrational frequencies, have been carried out on the optimized structure with the RDFT/B3LYP/6-31G (d) for the neutral state, and with UDFT/B3LYP/6-31G (d) for the doped state. Force constants were carried out by using the MOPAC 2009 program.[24]

The excited state was obtained by the re-optimization of the geometry by the configuration interaction singles restricted (RCIS) *ab initio* method (RCIS/STO-3G),[25] the transition energies for the excited state were calculated using TD-RDFT/B3LYP/6-31G (d). Results are compared with the available experimental data.

RESULTS AND DISCUSSION

Molecular chemical structure of PVK-3MeT copolymer

In our previous article,[13] we deduced from characterization studies a grafting mechanism between crosslinked PVK and PMeT. In the chemical synthesis, dissolved PVK and 3-methylthiophene monomers are present in a chemical environment rich on anhydrous $FeCl_3$ Lewis acids. In this condition, a chemical oxidative inter and intra crosslinking of the carbazole pendant groups in PVK occurred, inducing the formation of dimeric bicarbazilium radical cations.[13,26,27] In addition, the 3-methylthiophene monomer present in solution should be polymerized to form the poly(3-methylthiophene) main chain.[28] Finally, PMeT is grafted to the formed bicrabazole units. To make easy the paper to read, we briefly recall below this grafting mechanism (Scheme 1).

As mentioned before, we present in this article calculations based on DFT methodologies. Then, the obtained results will be compared with experimental characterization data[13] to deduce the molecular model that describes the best of the new copolymer and its properties. The proposed model is based on carbazole and 3-methylthiophene units. For theoretical data, we used the same hypothesis than that proposed in previous studies.[23,29–31] The most important approximation consists in assuming that the coupling of the radical-cation takes place by pairing the radical spin from each radical-cation to form a bond. In these conditions, the largest spin density value is more likely to form a bond via radical pairing. Calculated atomic spin densities of carbazole and 3-methylthiophene radical-cations are given in Scheme 2, obtained by using the UDFT/B3LYP/6-31G (d) calculations.

First, the analysis of the spin density distribution of carbazole moieties [Scheme 2(a)] shows that the

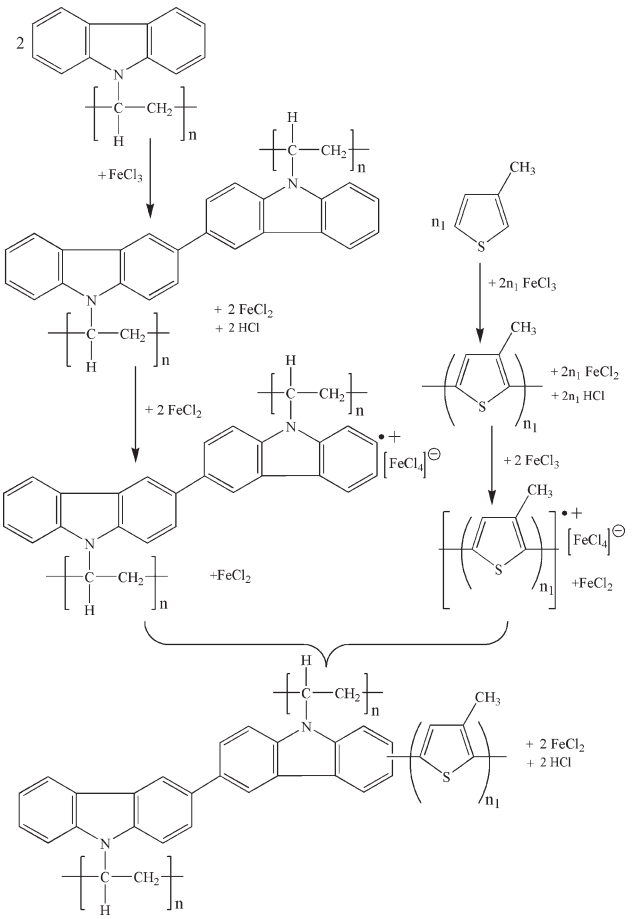

Scheme 1 Formation of PVK-3MeT graft copolymer.

high spin densities are localized on the three and six carbons of the carbazole moieties. This fact indicates that the coupling occurs preferentially at these atom sites under a chemical crosslinking of carbazole units in PVK backbone to form dimers of bicarbazilium units. This data is corroborated by experimental studies.[27,32]

On the second hand, the analysis of the spin density distribution of 3-methylthiophene units show that the high spin densities are located in carbon 2 or 5 of the thiophene rings [Scheme 2(b)]. This result lets us believe that the formation of PMeT main chain is created by the 2 or 5 coupling. In fact, it was shown that $FeCl_3$ generates essentially polymerization by two to five coupling and not by two to four coupling.[33] In addition, it is known that the polymerization with $FeCl_3$ leads in general to irregular poly(alkylthiophene) and approximately 70 to 80% of regular Head to Tail coupling is generated.[33] Based on NMR and XRD results,[13] the PMeT main chain in the synthesized copolymer is region-random and we estimate the regioregularity with a 70 to 80% of HT coupling.

For the bicarbazole dimer unit, the high spin density is located at carbons 1 and 8 (Scheme 3), which reveal that the grafting of PMeT main chain occurs preferentially at these sites for the bicabazole units.

Based on this consideration, we propose an oligomer model structure for the synthesized PVK-3MeT1 and PVK-3MeT2 graft copolymer by the grafting of six 3-methylthiophene units coupled at 2 or 5 positions, with a regiorandom configuration to a dimeric bicarbazole unit. The structure of studied molecules is sketched in Scheme 4.

DFT optimized molecular structure of PVK-3MeT

Geometrical and structural properties in the ground neutral state

First, the optimized configuration of the neutral ground state molecular structure was simulated by RDFT calculations, using the RB3LYP and RB3PW91 methods, combined with 6-31G (d) basis sets. All corresponding geometrical parameters such as bond lengths, inter-ring dihedral angles are collected respectively, in Figure 1 and Table I. Notice that no important variation in bond lengths was found in varying the method of simulation. From the inter-ring dihedral angles of the neutral ground state optimized configuration, we can conclude that the copolymer structure is nonplanar. It is obvious that the torsion angle constitutes a compromise between the effect of conjugation and the steric repulsion

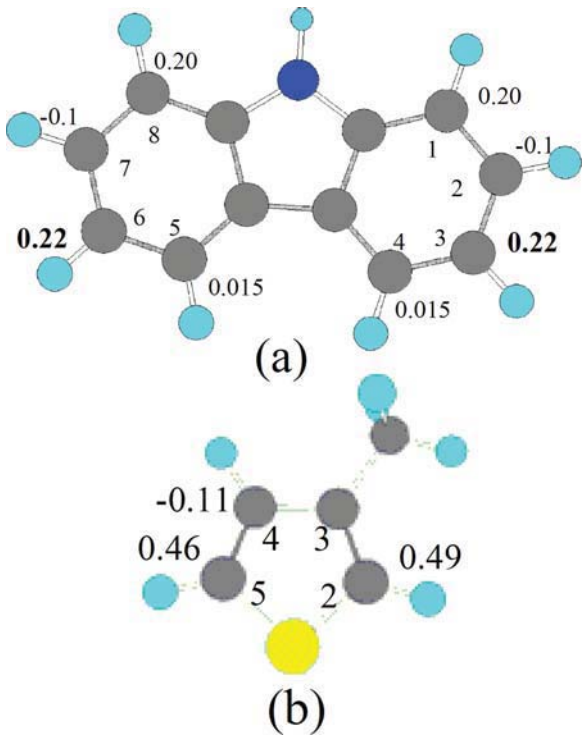

Scheme 2 Calculated total atomic spin densities of radical cations of: (a) carbazole and (b) 3-methylthiophene units. [Color figure can be viewed in the online issue, which is available at wileyonlinelibrary.com.]

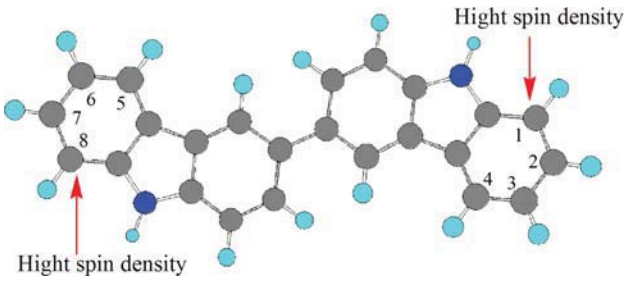

Scheme 3 Chemical structure of bicarbazole units by 3-3 coupling of carbazole units. [Color figure can be viewed in the online issue, which is available at wileyonlinelibrary.com.]

between hydrogen atoms, which favors a nonplanar structure.[34] The high inter-ring torsion is detected essentially between the two carbazole units forming the bicarbazole unit ($\Phi_1 = -39.0°$), and between the two non regular Tail to Tail coupled methylthiophene ($\Phi_5 = 56.4°$). In fact, it is known that a regular coupling HT-HT of thiophene rings induces a planar structure, while the presence of irregular coupling generates a distortion in the main chain, inducing a non planar structure and then a decrease on the effective conjugation length.[33]

Geometrical and structural properties in the doped state

Under chemical doping (oxidation) of the copolymer by $FeCl_3$, an electron transfer occurs from the copolymer backbone to $FeCl_3$ and $FeCl_4^-$ counter-anions is formed. These facts indicate that positive charges or holes are created on the copolymer backbone upon $FeCl_3$ oxidation.[35] The optimized configuration of the doped state molecular structure was simulated with the open shell system UDFT/B3LYP and UDFT/B3PW91 with the injection of a hole in the molecule. All geometrical parameters of the fully optimized molecular structure such as bond lengths and dihedral angles are respectively, collected in Figure 1 and Table I.

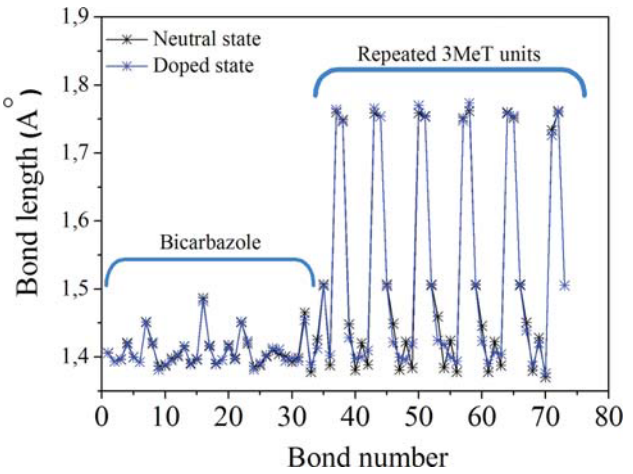

Figure 1 Bond lengths of the neutral and doped optimized structures as a function of bonds number. [Color figure can be viewed in the online issue, which is available at wileyonlinelibrary.com.]

Upon doping, geometrical parameters such as dihedral angles and bond lengths are greatly affected. First, we note that a great decrease of the inter-ring torsion Φ_3, Φ_4, Φ_5, Φ_6, and Φ_7 (see Table I), which favors a planar structure in the doped state. On the other hand, the injection of holes in this structure induces better conjugation than in its corresponding neutral ground state. From Figure 1, we can deduce that there is no variation of the bond lengths of the bicarbazole units, whereas altered units of 3-methylthiophene are characterized by a shortening of single bonds and lengthening of double ones.

Force constants are defined by $F_{RR'} = [\partial^2\Phi/\partial R\partial R']$, where Φ is the potential energy, R and R' are two internal coordinates. The semi empirical relationship between the carbon–carbon bond length and the corresponding stretching force constant is defined as: $F_{C\text{-}C} \propto (1/r_{cc}^4)$.[36] Force constants are collected in Figure 2. We can deduce no important modification in the force constants in the bicarbazolyl units of the oligomer, while important

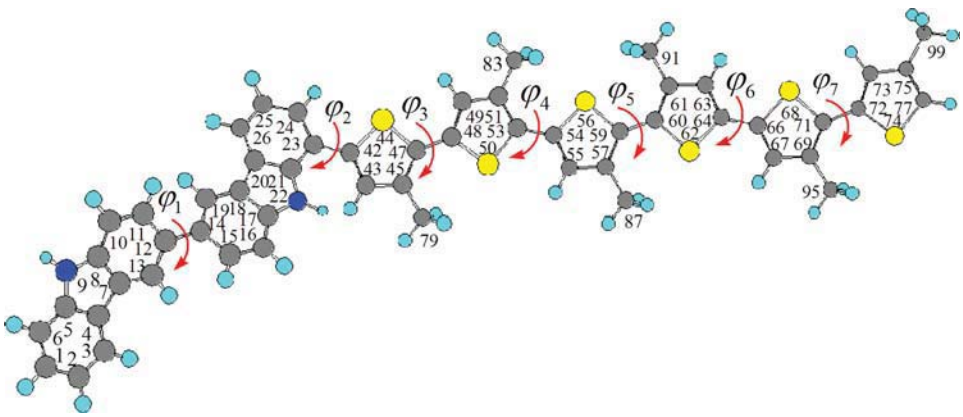

Scheme 4 Molecular structure of PVK-3MeT copolymer. [Color figure can be viewed in the online issue, which is available at wileyonlinelibrary.com.]

TABLE I
Inter-Ring Dihedral Angles of the Optimized PVK-3MeT Molecular Structure in the Neutral and Doped States

	Neutral state	Doped state	Neutral state	Doped state
Dihedral angle (°)	RB3LYP/6-31G (d)	UB3LYP/6-31G (d)	RB3PW91/6-31G (d)	UB3PW91/6-31G (d)
Φ_1	−39	−37.64	−40.25	−38.5
Φ_2	37	31.87	38.8	33.5
Φ_3	24.6	−3.9	−24	−4.47
Φ_4	12	0.67	27	0.64
Φ_5	56.4	0.47	60	0.72
Φ_6	12.2	−0.32	−15.9	−1.31
Φ_7	−23.3	0.28	−27.8	4.8

modifications are detected for the successive 3-methilthiophene rings. Then, the injection of holes in this oligomer tends to the formation of a quinoïdal structure localized at the methylthiophene rings. Consequently, the formation of polaronic charge carriers, which induce a planarity in the geometry of the oligomers backbone, can affect the conjugation. Accordingly, these features are a signature of a significant improvement in the properties of charge transport, explaining the high conductivity measured for PVK-3MeT1 in the doped (oxidative) state (0.21 S/cm) relative to that of the neutral state ($\sim 10^{-10}$ S/cm).[13]

Vibrational properties

Based on the fully optimized neutral ground and doped states oligomer structure, infrared and Raman spectra of the studied molecular structure are simulated by RDFT/B3LYP/6-31G (d) and DFT/UB3LYP/6-31G (d) for the neutral and doped states, respectively.

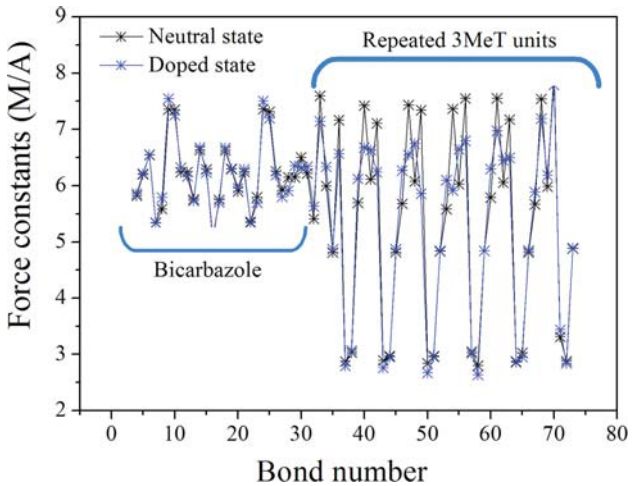

Figure 2 Force constants of the neutral and doped optimized structures as a function of bonds number. [Color figure can be viewed in the online issue, which is available at wileyonlinelibrary.com.]

In Figure 3, we show experimental normalized infrared spectrum of neutral PVK-3MeT1 [Fig. 3(a)], plotted with normalized simulated infrared spectrum of the neutral ground state PVK-3MeT molecular structure [Fig. 3(b)]. The experimental and theoretical frequencies and their complete assignments are collected in Table II.

In the experimental infrared spectrum of PVK-3MT1, we can distinguish firstly the characteristic vibration of carbazole groups and in particular, the

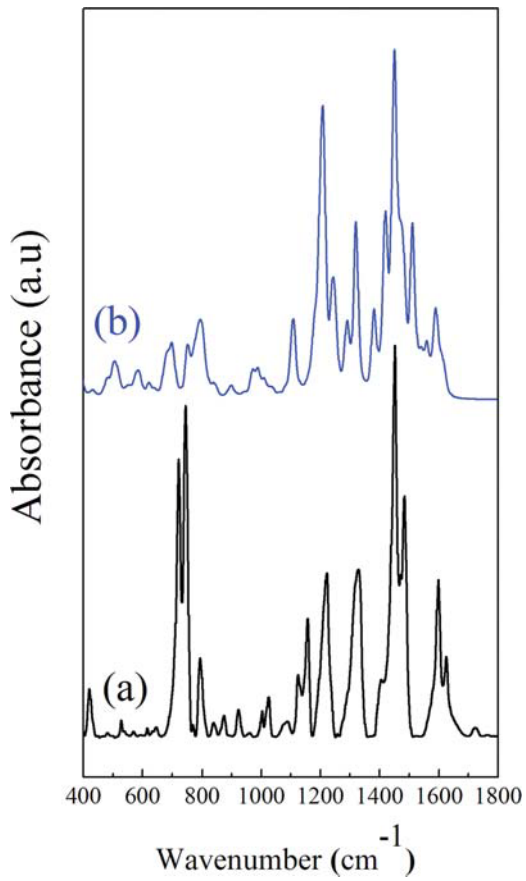

Figure 3 Experimental normalized infrared spectrum of neutral PVK-3MeT1 (a) and normalized simulated infrared spectrum of the neutral ground state PVK-3MeT molecular structure (b). [Color figure can be viewed in the online issue, which is available at wileyonlinelibrary.com.]

TABLE II
Infrared Experimental and Simulated Frequencies of PVK-3MeT1 for the Neutral and Doped States

PVK-3MeT1 (neutral state) experimental frequency (cm^{-1})	I	Calculated frequency (cm^{-1}) (neutral state) DFT/RB3LYP/6-31G (d)	I	PVK-3MeT1 (doped state) experimental frequency (cm^{-1})	Calculated frequency (cm^{-1}) (doped state) DFT/UB3LYP/6-31G (d)	Assignements[13,37–39]
727	M	700	w	720	–	C-H deformation in PVK
745	M	750	w	746	740	C-H deformation in PVK
790	W	797	w	790		1,2,4 Trisubstituted benzene nuclei
835	W	845	vw	830	830	Aromatic C-H out of plane deformation in PMeT
880	W	900	w	864	870	C-S stretching vibration in PMeT
930	W	970	w	–	–	C-C deformation in PVK
				970	1085	Doping induced band
1010	W	1010	w	1010	1010	C-C deformation in PVK
1025	W	1020	w	1025	1050	C-C deformation in PVK
1122	M	1110	m	–	–	–
1163	M	–	–	1157	1170	C-C deformation in PVK/doping induced band
1225	M	1210	s	1210	1250	C-N stretching in PVK
–	–	–	–	1310	1310	Doping induced band
1315	M	1320	m	–	–	C-H deformation in PVK
1380	W	1380	w	1390	1380	CH_3 deformation in PMeT
1450	S	1450	s	1450	1440	C-H deformation in PVK/doping induced band
1480	S	1510	s	1480	1480	CH_2 rocking vibration in PVK
1600	M	1560	w	1600	1640	CH_2 rocking vibration in PVK
1625	M	1590	m	1625	1660	Ring vibration of VK moiety in PVK/ring stretching in thiophene moiety

w: weak; vw: very weak; m: mean; s: strong.

vibration at 790 cm^{-1} characteristic of the 1,2,4 trisubstituted benzene nuclei reflecting the crosslinking of PVK. This results suggest the formation of dimeric bicarbazylium through the 3/6 carbazole radical coupling.[37] Meanwhile, we can distinguish the vibrations of poly (3-methylthiophene) at 830, 880, 1400, and 1625 cm^{-1} which prove the formation of the PMeT main chain, in particular the vibration at 830 cm^{-1} due to the two to five coupling 3-methylthiophene, while no peaks are detected for the two to four coupling at 730 and 840 cm^{-1}. Again this demonstrates further the coupling of 3-methylthiophene through two to five coupling.[38,39]

Experimental Raman spectrum of de-doped PVK-3MeT1 [Fig. 4(a)] is dominated essentially by an intense peak at 1450 cm^{-1}. It is assigned to the $C_\alpha = C_\beta$ ring stretching of the aromatic PMeT structure,[40] showing the successful de-doping of the sample under the chemical treatment. In simulated Raman spectrum, this peak is up shifted to 1500 cm^{-1} [Fig. 4(b)].

It is worth noticing that experimental Infrared and Raman spectra of de-doped PVK-3MeT1 reproduce the main vibrations of the proposed molecular structure. The calculated frequencies agree well with those experimental values. Then, deviations of about 5 to 10 cm^{-1} and 20 to 50 cm^{-1} are obtained for

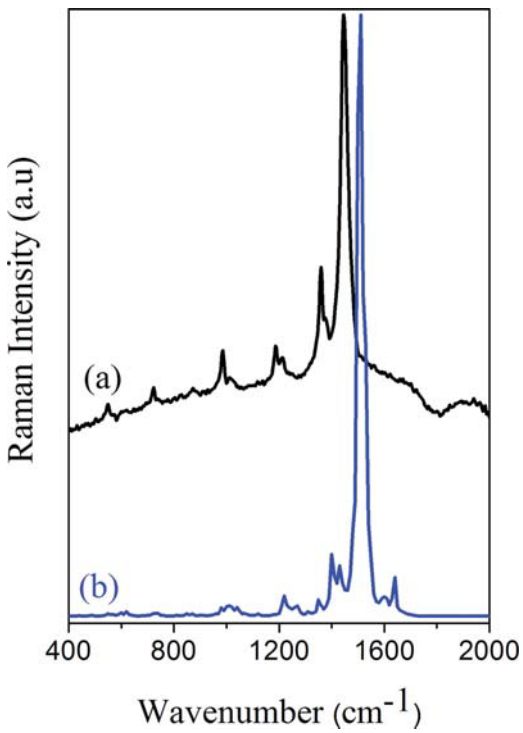

Figure 4 Experimental Raman spectrum of de-doped PVK-3MeT1 (a) and simulated Raman spectrum PVK-3MeT molecular structure (b). [Color figure can be viewed in the online issue, which is available at wileyonlinelibrary.com.]

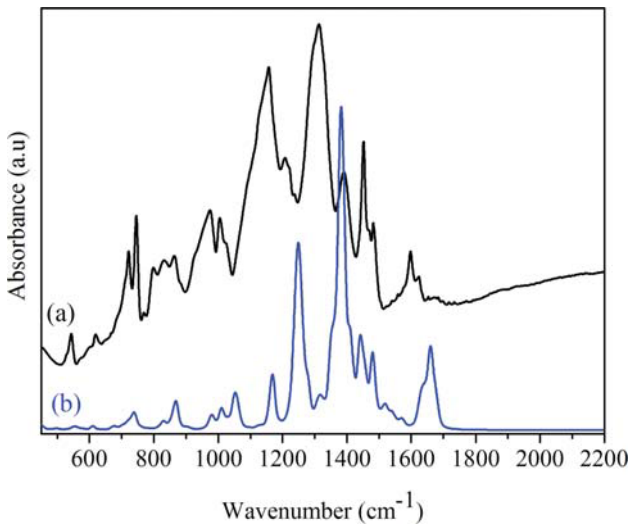

Figure 5 Normalized experimental and UDFT simulated infrared spectra of doped PVK-3MeT1 (a) and PVK-3MeT (b). [Color figure can be viewed in the online issue, which is available at wileyonlinelibrary.com.]

infrared and Raman vibrational spectra, respectively. This confirms the choice of the molecular structure for the new synthesized PVK-3MeT graft copolymer.

In Figure 5, we present normalized experimental and UDFT simulated infrared spectra of doped PVK-3MeT1 [Fig. 5(a)] and PVK-3MeT [Fig. 5(b)] samples, respectively. The doping effect, which is clearly seen in infrared spectra, supported by the appearance of strong peaks at 970, 1150, and 1320 cm^{-1}, as a the signature of the oxidation of PMeT main chain by the formation of quinoid structure.[41] This effect is supplementary confirmed in simulated infrared spectrum of the doped PVK-3MeT obtained by DFT/UB3LYP/6-31G (d).

Frontier molecular orbitals (HOMO and LUMO)

It may be useful to examine the highest occupied and the lowest unoccupied orbital Molecular (HOMO and LUMO) for this oligomer and copolymer, to obtain information about the HOMO and the LUMO distribution of the compound, in its neutral and doped states. To gain information on the difference in the electronic properties between the pristine and the doped state, of the prepared graft copolymer, we have plotted the frontier orbitals of HOMO and LUMO for the fully optimized neutral and that of the fully doped states in Figure 6(a,b), respectively. As shown in Figure 6(a), the frontier orbitals distributing in the neutral PVK-3MeT spread over the whole π-conjugated backbone. In general, the HOMO is expected to lie on the electron-rich groups. Frontier orbitals HOMO and LUMO for the neutral state [Fig. 6(a)] are mainly localized on the coupled 3-methylthiophene units. There is antibonding between the bridge atoms of the inter-ring, and there is bonding between the bridge carbon atom and joint atoms of the intraring in the HOMO. On the contrary, there is bonding in the bridge single bond of the inter-ring and the antibonding between the bridge atoms and its neighbor of the intraring in the LUMO. In general, the HOMO possesses an antibonding character between the subunits.[42] This may explain the no-planarity observed for this oligomer in their ground neutral state. On the other hand, the LUMO generally shows a bonding character between the two adjacent subunits.[42] Upon doping, the injection of holes in these oligomers involves dramatic changes in the geometrical and vibrational properties, inducing a high modification in the electronic properties and especially in the HOMO and LUMO distributions. In Figure 6(b), we present HOMO and LUMO distributions of doped PVK-3MeT. Dramatic changes in the HOMO and LUMO are also observed upon doping. It consists essentially on the change of the localization of the electronic clouds of HOMO from the repeated 3-methylthiophene units in the neutral state to the coupled bicarbazole unit. The HOMO and LUMO energies

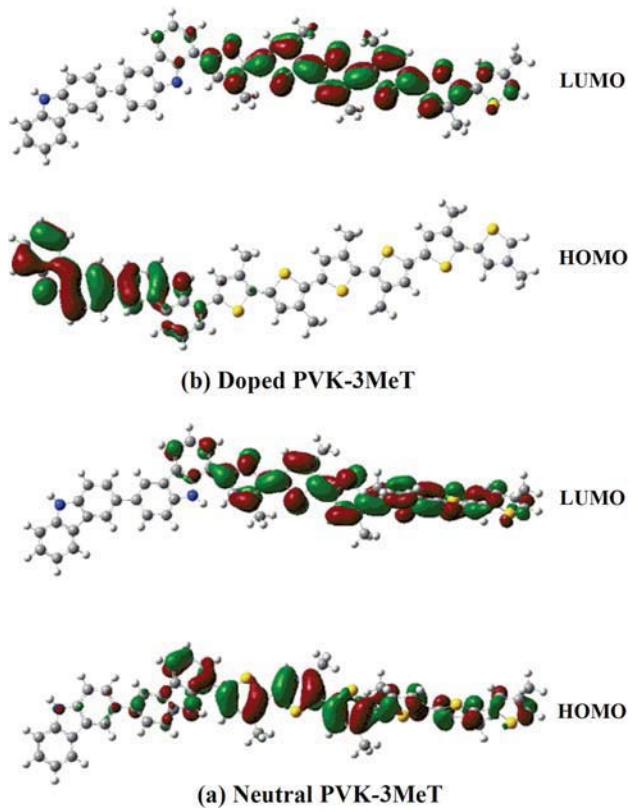

Figure 6 The contour plots of HOMO and LUMO orbitals of (a) neutral and (b) doped states of PVK-3MeT. [Color figure can be viewed in the online issue, which is available at wileyonlinelibrary.com.]

TABLE III
Simulated and Experimental Optoelectronic Parameters in the Neutral and Doped States (E_g, IP, EA)

		DFT calculated values					Experimental optical band gap (E_g, eV)[13]		
		ε_{HOMO} (eV)	ε_{LUMO} (eV)	E_g (*eV*)	IP (eV)	EA (eV)	PVK-3MeT2 (chloroform solution)	PVK-3MeT2 (disposed thin cast film)	PVK-3MeT1 (condensed state)
Neutral state RDFT	RB3LYP	−4.83	−1.79	3.00	4.83	1.83	2.5–2.6	2.6–2.7	–
	RB3W91	−4.98	−1.82	3.10	4.98	1.88			
Doped state UDFT	UB3LYP	−6.49	−4.59	1.90	–	–	–	–	1.9
	UB3W91	−6.60	−4.66	1.94	–	–			

(ε_{HOMO}, ε_{LUMO}) are calculated accurately by DFT and presented in Table III.

Optical properties

Absorption spectra

UV-Vis absorption and emission spectra of de-doped PVK-3MeT2 and optical absorption spectra of doped PVK-3MeT1 were reported in our previous study.[13]

The deconvolution of the optical absorption spectra of de-doped PVK-3MeT2 in the solid state and in solution into components of Lorentzien profiles shows that the sample absorbs at 430, 330, 270, and 240 nm in the solid state and at 410, 330, 270, and 240 nm in solution.[13] Meanwhile, the deconvolution of the optical absorption spectra of doped PVK-3MeT1 in the range 200 to 650 nm shows that PVK-3MeT1 absorbs in the UV part of the electromagnetic spectrum with bands centered at 240, 310, and 360 nm and in the visible part with another band centered at around 440 nm. Moreover, the decomposition of the optical absorption spectra of doped PVK-3MeT1 for wavelengths between 600 and 3000, into components of Lorentzien profiles, show absorption transitions in the doped state at 830, 1450, and 1950 nm.[13]

It is shown by Gierschner et al.[43] that experimental optical band gap (E_g) of organic compounds can be easily determined experimentally as the energy at the intersection of the normalized fluorescence and absorption spectra. Experimental optical band gap of neutral PVK-3MeT2 in solution is estimated to 2.5 eV while that of PVK-3MeT2 cast film is estimated to 2.6-2.7 e V.[13] For doped PVK-3MeT1, the optical band gap can be deduced from the normalized absorption spectra by the following formula $E_g = 1240/\lambda_{onset}$, when the onset of absorption is deduced from the absorption spectrum by the extrapolation of the linear JI-JI* part of the spectrum. Experimental optical band gap (E_g) is estimated for doped PVK-3MeT1 to be 1.9 e V.[13]

Theoretically, the calculated band gap is estimated from the energy difference between the HOMO and LUMO energy levels.[43] Theoretical data such as ε_{HOMO}, ε_{LUMO}, IP, EA, $E_g = \varepsilon_{HOMO} - \varepsilon_{LUMO}$, and experimental optical band gap are listed in Table III. All calculations were performed with the basis set of 6-31G (d).

Based on fully DFT optimized structure of the ground neutral and doped states of oligomer, theoretical transition energies were calculated using time-dependent density functional theory (TD-DFT)

TABLE IV
Simulated and Experimental Electronic Transitions in the Neutral State, Calculated Oscillator Strengths

	Experimental wavelength[13]		TD-RDFT calculated transition				
			RB3LYP		RB3PW91		
Electronic transition	Solution (nm /eV)	Disposed cast thin film (nm /eV)	6-31G (d) (nm /eV)	*f*	6-31G (d) (nm /eV)	*f*	MO/character
$S_0 \rightarrow S_1$	410 /3.02	430/ 2.88	465/ 2.67	2.14	446/ 2.77	2.08	H→L (+87%)
$S_0 \rightarrow S_2$	330/3.75	330/ 3.75	376/ 3.29	0.36	368/ 3.36	0.35	H-1→L + 1 (+78%)
$S_0 \rightarrow S_3$	270/4.59	270/4.59	294/4.21	0.16	273/4.53	0.16	H-1→L + 5 (+19%). H→ L +.6 (+17%). H-7→L (11%). H-2 →L + 4 (10%) H-5→L + 1 (7%). H-1→L + 4 (+7%)
$S_0 \rightarrow S_4$	240/5.16	240/5.16	261/4.75	0.11	254/4.87	0.2	H-5→L + 3 (+31%). H-3→L + 4 (+8%). H-4→L (+8%). H-2→L + 5 (+5%)

f: Oscillator strength.

TABLE V
Simulated and Experimental Electronic Transitions in the Doped State of PVK-3MeT

TD-UDFT calculated transition (doped state)				
UB3LYP/6-31G (d) (nm /eV)	*f*	UB3PW91/6-31G (d) (nm /eV)	*f*	Experimental wavelength[13] (nm /eV)
3789.50/0.3272	0.3392	3753.95/0.3303	0.3461	–
1935.23/0.6407	0.0271	1905.51/0.6507	0.0307	1970/0.63
1467.59/0.8448	0.4284	1458.87/0.8499	0.4377	1450/0.85
805.60/1.5390	0.7073	790.41/1.5686	0.7150	830/1.49
465.00/2.6663	0.0236	460.28/2.6936	0.0282	450/2.75
361.29/3.4317	0.0590	340.55/3.6407	0.0446	350/3.54
303.47/4.0856	0.0317	319.52/3.8804	0.0421	300/4.13
267.04/4.6429	0.3040	270.85/4.5777	0.1816	240/5.16

f: Oscillator strength.

method, and it provides a good predictive tool for absorption spectra of molecules. Electronic transitions, oscillator strengths excitation and M/O characters are listed in Tables IV and V with experimental optical transitions respectively, for the neutral and doped states.

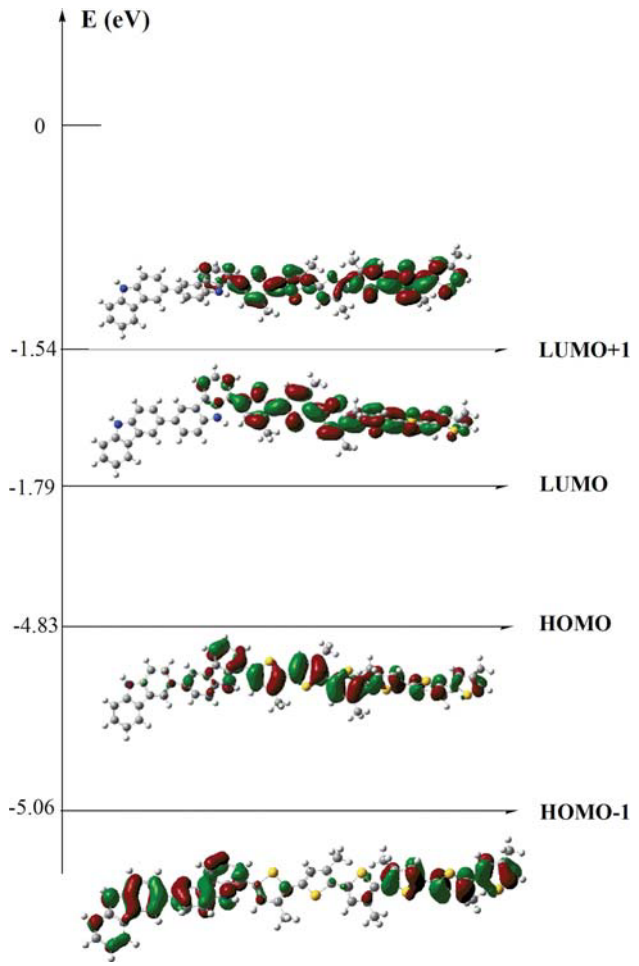

Figure 7 TD-DFT electronic structure of the synthesized copolymer for the neutral state. [Color figure can be viewed in the online issue, which is available at wileyonlinelibrary.com.]

For the PVK-3MeT copolymer studied in this work, both $E_g = \varepsilon_{HOMO} - \varepsilon_{LUMO}$ approach and TD-DFT excitation energies are in good agreement with experimental results (see Tables III–V), even if small discrepancies still exist. In fact, two factors may be responsible for small deviations detected by used theoretical methods from experimental data. First, the predicted band gap and the excitation energies are performed by DFT and TD-DFT approaches for the isolated gas-phase chain, while the experimental band gaps are measured in the liquid or condensed phase and the solvent shift can be estimated to be 0.1 to 0.3 eV.[43] Second, we should keep in mind that solid-state effects (like polymerization effects and intermolecular packing forces) have been neglected in the calculations. Therefore, we can conclude that the theoretical band gap and excitation energies agree with the experimental optical properties of the PVK-3MeT synthesized copolymer.

The $S_0 \rightarrow S_1$ transition in PVK-3MeT in the neutral state occurs with high intensity of the oscillator strength calculated (see Table V). This high value indicates an important photoabsorption degree, while $S_0 \rightarrow S_2$, $S_0 \rightarrow S_3$, and $S_0 \rightarrow S_4$ induce much weaker photoabsorption. This is in good agreement with the experimental optical absorption spectra of neutral PVK-3MeT2. The electronic structure of the synthesized copolymer for the neutral state, deduced from the simulated TD-DFT is presented in Figure 7.

Properties and emission spectra of excited structures

Density functional methods are, however, not able to provide a geometry optimization in the excited states because of a lack of efficient algorithms for analytical gradients. Up to now, the standard for calculating excited state equilibrium properties of larger molecules is the Restricted Configuration Interaction Singles (RCIS) *ab initio* method.[16] In this study, our

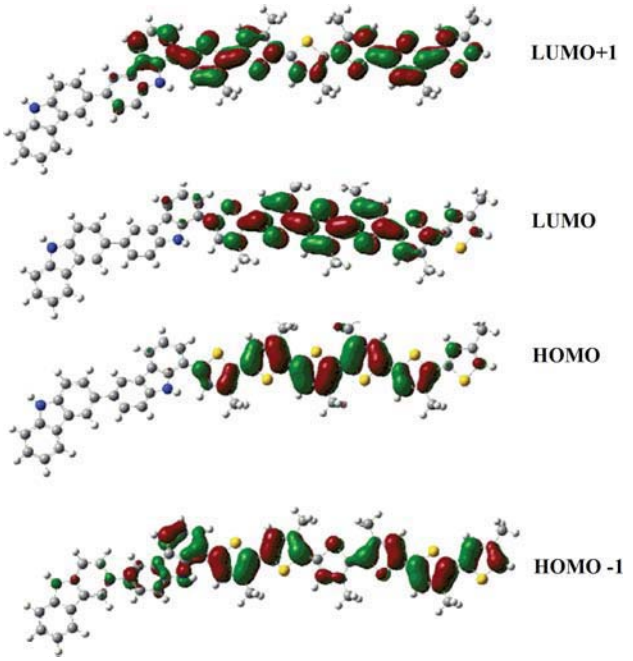

Figure 8 Frontier orbitals of HOMO and LUMO for the fully optimized excited structure of neutral state of PVK-3MeT. [Color figure can be viewed in the online issue, which is available at wileyonlinelibrary.com.]

goal is to investigate the excited-state properties using this method. Because the studied PVK-3MeT molecular structure is a large molecule which is a constraint of the calculation of the excited state, we optimize the PVK-3MeT molecular structure for the excited state by RCIS/STO-3G.

Under excitation, we find essentially a reduction of the dihedral inter-ring angle between the coupled 3-methylthiophene Φ_3,Φ_4, Φ_5, Φ_6, Φ_7, from 24.6, 12, 56.4, 12.2, −23.3° in the ground neutral state obtained by DFT/RB3LYP/6-31G (d) to −0.82, 0.02, −0.015, 0.003, −0.006° respectively, in the excited state. Whereas, no important reduction is found for the inter-ring dihedral angle Φ_1 between the dimer of carbazole from −39° in the ground neutral state to −39.189° in the excited state. A similar result is obtained for the dihedral angle between carbazole and 3-methylthiophene unit Φ_2 from 37° in the neutral ground state to 30.37 in the excited state. It is obvious that the excited structure has a strong planar tendency, with a better conjugation, which further corroborates the predictions from frontier orbital's (Fig. 8).

Experimental emission spectra of PVK-3MeT1 are investigated in powder. The sample was excited at 450 nm. However, emission spectra of PVK-3MeT2 are investigated in chloroform solution and in solid cast films at room temperature for excited wavelengths at 380 and 450 nm. The experimental fluorescence spectrum of PVK-3MeT2 displays a maximum emission at 570 nm in solution and at 628 nm in solid cast film with excitations at 380 and 450 nm,[13] respectively. On the other hand, the experimental fluorescence emission of PVK-3MeT1 in powder displays a maximum emission maximum at 573 nm.[13]

The emission calculations are made by re-optimizations of the PVK-3MeT molecular structure with the RCIS/STO-3G method in its singlet excited state, followed by using the resulting geometry to perform TD calculations employing RB3LYP/6-31G (d) method in the gas phase. The $S_0 \rightarrow S_1$ fluorescence peaks at 571.79 nm has the strongest oscillator intensity (2.6157) arising from HOMO to LUMO π-π* excitation, in close agreement with the experimental emission of PVK-3MeT2 in solution (570 nm) and that of PVK-3MeT1 in powder (573 nm). The fluorescence of PVK-3MeT2 in solid cast films red-shifted compared to their corresponding samples in solution or gas phase. This can be explained by the more planar conformation in the cast film, which increases the degree of conjugation in the polymer backbone.[44] Notice that the simulated fluorescence of PVK-3MeT molecular structure was done by TD-DFT in gas phase. In Figure 9, we present together experimental normalized fluorescence spectra of PVK-3MeT1 obtained in powder and that of PVK-3MeT2 obtained in solution and in solid cast films, and normalized simulated fluorescence spectra of PVK-3MeT molecular structure calculated from the

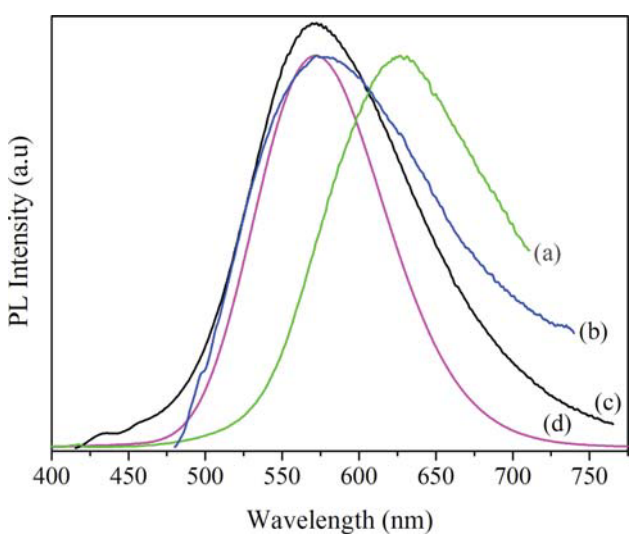

Figure 9 Experimental PL spectra of: PVK-3MeT2 investigated in disposed cast films (a) (excitation 380 nm), PVK-3MeT1 investigated in powder (b) [powder was collected between two silica plates and excited at 450 nm], PVK-3MeT2 in chloroform solution (excitation 380 nm) (c) and simulated PL spectrum of the studied PVK-3MeT molecular structure obtained by TD-DFT/RB3LYP/6-31G (d) based on the optimized excited state obtained by RCIS/STO-3G (d). [Color figure can be viewed in the online issue, which is available at wileyonlinelibrary.com.]

excited state by TD-DFT and transformed by Swizard program.[45]

Ionization potentials and electron affinities

Based on the Koopman's theorem,[46] the ionization potential IP is estimated to be the negative of the highest occupied molecular orbital (HOMO) energy ($IP = -\varepsilon_{HOMO}$), while the electron affinity (EA) can be determined from the difference between the band gap and the ionization potential.[47] The ionization potential (IP) in the PVK-3MeT copolymer is estimated to be 4.83 eV, lower than (around 0.4 eV) that of homo-polymer PMeT (5.2 eV).[47] Moreover the electron affinity of PVK-3MeT is estimated to be 1.8 eV, lower than that of homo-polymer PMeT (3.92 eV).[47]

CONCLUSIONS

We have presented a theoretical model for the new prepared graft copolymer PVK-3MeT in neutral, doped and excited states. Our calculations suggest a good agreement between excitation energies obtained by TD-DFT calculations and the optical properties obtained from experimental data. The theoretical simulation based on DFT methodologies on the molecular structure helped to provide a description of the geometry and of the optoelectronic properties of the new synthesized copolymer. Upon doping, we observe essentially an enhancement of the planarity which induces a great modification in the cloud distribution in the HOMO and LUMO orbital's and consequently, a large modification in its electronic structure. Finally, this study confirms experimental data and shows that the changes of structure could greatly modulate and improve the electronic and optical properties of the pristine polymer. Furthermore, we showed that it is possible to predict reasonably the electronic properties of organic systems and help to understand the structure-properties relationship of these materials.

Authors are grateful to Mr. Jean-Pierre Boulard for the authorization access to the CCIPL (Intensive Computing center at the University of Nantes (Pays de la Loire)).

References

1. Lefrant, S.; Baibarac, M.; Baltog, I.; Godon, C.; Mevellec, J. Y.; Wéry, J.; Faulques, E.; Mihut, L.; Aarab, H.; Chauvet, O. Synth Met 2005, 155, 666.
2. Matuszna, K.; Lukes, V.; Rapta, P.; Dunsch, L.; Aquino, A.; Lischka, H. Synth Met 2007, 157, 214.
3. Péres, L. O.; Wang, S. H.; Wéry, J.; Froyer, G.; Faulques, E. J Mater Sci Eng C 2009, 29, 372.
4. Ayachi, S.; Alimi, K.; Bouachrine, M.; Hamidi, M.; Mevellec, J. Y.; Lère-Porte, J. P. Synth Met 2006, 156, 318.
5. Tzamalis, G.; Lemaur, V.; Karlsson, F.; Holtz, P.; Andersson, M.; Crispin, X.; Cornil, J.; Berggren, M. Chem Phys Lett 2010, 489, 92.
6. Faulques, E.; Ivanov, V. G.; Jonusauskas, G.; Athalin, H.; Pyshkin, O.; Wéry, J.; Massuyeau, F.; Lefrant, S. Phys Rev B 2006, 74, 075202.
7. Wéry, J.; Aarab H., Lefrant, S.; Faulques, E.; Mulazzi, E.; Perego, R. Phys Rev B 2003, 67, 115202.
8. Akcelrud, L. Prog Polym Sci 2003, 28, 875.
9. Andersson, M. R.; Thomas, O.; Mammo, W.; Svensson, M.; Theander, M.; Ingana, O. J. J Mater Chem 1933 1999, 9.
10. Mabrouk, A.; Alimi, K.; Molinie, P.; Nguyen, P. J Phys Chem B 2006, 110, 1141.
11. Ayachi, S.; Bouzakraoui, S.; Hamidi, M.; Bouachrine, M.; Molinie, P.; Alimi, K. J Appl Polym Sci 2006, 100, 57.
12. Aouchiche, H. A.; Djennane, S.; Boucekkine, A. Synth Met 2004, 140, 127.
13. Chemek, M.; Wéry, J.; Bouachrine, M.; Paris, M.; Lefrant, S.; Alimi, K. Synth Met 2010, 160, 2306.
14. Pesant, S.; Boulanger, P.; Cotea, M.; Ernzerhof, M. J Chem Phys Lett 2008, 450, 329.
15. Frisch, M. J.; Trucks, G. W.; Schlegel, H. B.; Scuseria, G. E.; Robb, M. A.; Cheeseman, J.; Montgomery, J A.,Jr.; Vreven, T.; Kudin, K. N.; Burant, J. C.; Millam, J. M.; Iyengar, S. S.; Tomasi, J.; Barone, V.; Mennucci, B.; Cossi, M.; Scalmani, G.; Rega, N.; Petersson, G. A.; Nakatsuji, H.; Hada, M.; Ehara, M.; Toyota, K.; Fukuda, R.; Hasegawa, J.; Ishida, M.; Nakajima, T.; Honda, Y.; Kitao, O.; Nakai, H.; Klene, M.; Li, X.; Knox, J. E.; Hratchian, H. P.; Cross, J. B.; Adamo, C.; Jaramillo, J.; Gomperts, R.; Stratmann, R. E.; Yazyev, O.; Austin, A. J.; Cammi, R.; Pomelli, C.; Ochterski, J. W.; Ayala, P. Y.; Morokuma, K.; Voth, G. A., Salvador, P.; Dannenberg, J. J.; Zakrzewski, V. G.; Dapprich, S.; Daniels, A. D.; Strain, M. C.; Farkas, O.; Malick, D. K.; Rabuck, A. D.; Raghavachair, K.; Foresman, J. B.; Ortiz, J. V.; Cui, Q.; Baboul, I.; Martin, R. L.; Fox, D. J.; Keith, T.; Al-Laham, M. A.; Peng, C. Y.; Nanayakkara, A.; Challacombe, M.; Gill, P. M. W.; Johnson, B.; Chen, W.; Wong, M. W.; Gonzalez, C.; Pople, J. A. Gaussian 03, Revision B. 04; Gaussian, Inc.: Pittsburgh, PA, 2003.
16. Yang, L.; Feng, J.; Ren, A. J Comput Chem 2005, 26, 969.
17. Belletete, M.; Beaupre, S.; Bouchard, J.; Blondin, P.; Leclerc, M.; Durocher, G. J. J Phys Chem B 2000, 104, 9118.
18. Lee, C.; Yang, W.; Parr, R. G. J Phys Rev B 1998, 37, 785.
19. Becke, A. D. J Chem Phys 1996, 104, 1040.
20. Becke, A. D. J Chem Phys 1993, 98, 1372.
21. Perdrew, J. P.; Wang, Y. J Phys Rev 1992, 45, 13244.
22. Casado, J.; Katz, H. E.; Hernandez, V.; Lopez, J. Vib Spectrosc 2002, 30 175.
23. Ando, S.; Ueda, M. Synth Met 2002, 129, 207.
24. Stewart, James J. P. (2009), "Stewart Computational Chemistry, Version 9.126W", web: http://OpenMOPAC.net.
25. Belletête, M.; Bedard, M.; Leclerc, M.; Durocher, G. J. Mol Struct (Theochem) 2004, 679, 9.
26. Biswas, M.; Ballav, N. Synth Met 2003, 132, 213.
27. Maity, A.; Biswas, M. J Appl Polym Sci 2006, 100, 819.
28. Niemi, V. M; Knuuttila, P.; Österholm, J. E.; Korvola, J. Polymer 1992, 33, 1559.
29. Inagi, S.; Fuchigami, T. Synth Met 2008, 158, 782.
30. Fouad, I.; Mechbal, Z.; Chane-Ching, K.; Adenier, A.; Maurel, F.; Aaron, J.; Vodicka, P.; Cernovska, K.; Kozmik, V.; Svoboda, J. J Mater Chem 2004, 14, 1711.
31. Lo, C.; Adenier, A.; Chane-Ching, K.; Maurel, F.; Aaron, J.; Kosata, B.; Svoboda, J. Synth Met 2006, 156, 256.
32. Romero, D. B.; Schaer, M.; Leclerc, M.; Ades, D.; Siove, A.; Zuppiroli, L. Synth Met 1996, 80, 271.
33. Mc Cullough, R. D. Adv Mater 1998, 10, 93.
34. Faulgnes, E.; Wallufer, W.; Kuzmany, H. J Chem Phys 1989, 90, 7585.
35. Singh, R. K.; Kumar, J.; Singh, R.; Kant, R.; Chand, S.; Kumar, V. J Mater Chem Phys 2007, 104, 390.

36. Mabrouk, A.; Alimi, K.; Hamidi, M.; Bouachrine, M.; Molinie, P. Polymer 2005, 46, 9928.
37. Li, Y.; Yang, J.; Xu, J. J Electroanal Chem 1995, 399, 79.
38. Maior, S.; Wud, F. Synth Met 1989, 28, 281.
39. Pang, Y.; Xu, H.; Li, X.; Ding, H.; Cheng, Y.; Shi, G.; Jin, L. J Electrochem Commun 2006, 8, 1757.
40. Chen, F.; Shi, G.; Zhang, J.; Fu, M. Thin Solid Films 2003, 424, 283.
41. Chazaro-Ruiz, L.; Kellenberger, A.; Dunsch, L. J Phys Chem B 2009, 113, 2310.
42. Li, J.; Feng, J. K.; Ren, A. M. J Phys Org Chem 2009, 22, 118.
43. Gierschner, J.; Cornil, J.; Egelhaaf, H. Adv Mater 2007, 19, 173.
44. Ng, S. C.; Xu, J. M.; Chan, H. S. O. Synth Met 1998, 92, 33.
45. Gorelsky, S. SWizard Program; University of Ottawa: Ottawa, Canada, 2009.
46. Armelin, E.; Bertran, O.; Estrany, F.; Salvatella, R.; Alemán, C. Eur Polym Mater 2009, 45, 2211.
47. Vardhanan, R.; Zhou, L.; Gao, Z. Thin Solid Films 1999, 350, 283.